Research Square

Preprints are preliminary reports that have not undergone peer review.
They should not be considered conclusive, used to inform clinical practice,
or referenced by the media as validated information.

AI-guided Autonomous Workflows Accelerate Kinetic Analysis of Polymer Depolymerization

Tomonori Saito

saitot@ornl.gov

Oak Ridge National Laboratory https://orcid.org/0000-0002-4536-7530

Nicholas Galan

Oak Ridge National Laboraory

Britney Baez

Oak Ridge National Laboraory

Ju-An Kim

Oak Ridge National Laboraory

Beibei Yao

Oak Ridge National Laboraory

Nduka Ogbonna

Oak Ridge National Laboraory

Isaiah Dishner,

Oak Ridge National Laboraory

Jared Bowman

Oak Ridge National Laboraory

Jesse McGaha

Oak Ridge National Laboraory

Ankit Shrivastava

Oak Ridge National Laboraory

Stephen DeWitt

Oak Ridge National Laboraory

Sheng Dai

Oak Ridge National laboratory https://orcid.org/0000-0002-8046-3931

Craig Bridges

Oak Ridge National Laboratory https://orcid.org/0000-0002-3543-463X

Jeffrey C. Foster

ORNL https://orcid.org/0000-0002-9097-8680

Physical Sciences - Article

Keywords:

Posted Date: March 31st, 2026

DOI: https://doi.org/10.21203/rs.3.rs-9182434/v1

License: This work is licensed under a Creative Commons Attribution 4.0 International License.
Read Full License

Additional Declarations: There is **NO** Competing Interest.

AI-guided Autonomous Workflows Accelerate Kinetic Analysis of Polymer Depolymerization

Nicholas J. Galan,[1] Britney Baez,[1] Ju-An Kim,[1] Beibei Yao,[1] Nduka Ogbonna,[1] Isaiah Dishner,[1] Jared Bowman,[1] Jesse McGaha,[2] Ankit Shrivastava,[2] Stephen DeWitt,[2] Sheng Dai,[1] Craig Bridges,[1] Jeffrey C. Foster,[1] Tomonori Saito[1]

[1]Chemical Sciences Division, Oak Ridge National Laboratory, Oak Ridge, TN 37831, United States

[2]Computing and Computational Sciences Division, Oak Ridge National Laboratory, Oak Ridge, TN 37831, United States

Corresponding Authors: Tomonori Saito, saitot@ornl.gov; Jeffrey Foster, fosterjc@ornl.gov: Craig Bridges, bridgesca@ornl.gov

This manuscript has been authored by UT-Battelle, LLC, under contract DE-AC05-00OR22725 with the US Department of Energy (DOE). The US government retains and the publisher, by accepting the article for publication, acknowledges that the US government retains a nonexclusive, paid-up, irrevocable, worldwide license to publish or reproduce the published form of this manuscript, or allow others to do so, for US government purposes. DOE will provide public access to these results of federally sponsored research in accordance with the DOE Public Access Plan

Abstract

Deep understanding of polymerization and depolymerization kinetic behavior enables precision synthesis and manufacturing. However, traditional kinetic experiments are bottlenecked by labor-intensive sample collection and analysis practices and suffer reproducibility challenges due to human error and bias. Here, we introduce an artificial intelligence (AI)-driven automated kinetics platform to facilitate kinetic analysis and produce large volumes of high-quality kinetic data with minimal human intervention. Our autonomous workflow, encompassing automated synthesis, analysis, and cloud computing capabilities navigated complex parameter space using an importance-guided Bayesian optimization algorithm, effectively reducing sampling burden while maintaining accuracy in calculating apparent reaction rate constants. Kinetic data from these experiments supported the development of a stochastic simulation model to extract valuable mechanistic information. These capabilities were exploited for "scale-up" synthesis by conducting automated reactions in parallel, facilitating reproducible access to highly precise polymeric building blocks and providing a powerful alternative to polycondensation for the synthesis of telechelics by depolymerization. This work demonstrates how the throughput and accuracy of kinetic experiments can be significantly enhanced by synergizing AI and automation, highlighting the significant potential of these tools to transform the practice of fundamental polymer science.

Introduction

Next-generation polymeric materials integrate complex structural features such as specific chemical sequences and architectures to address emerging challenges in rare earth element recovery, microelectronics, intelligent matter, energy storage and conversion, and quantum computing.[1-7] Achieving the required level of synthetic control involves mastering reaction kinetics to manage the time-dependent nature of competing chemical processes during polymer synthesis, modification, or depolymerization. Advanced knowledge and synthetic tools are continuing to grow in this area and are essential for tailoring functional materials that deliver the necessary high-level performance.

One of the major limiting factors in the creation of next-generation materials is achieving precise molecular weight (MW) control during depolymerization. Waste polymers provide an abundant feedstock to produce new materials,[8-11] and the properties of these upcycled polymers inherently depend on the molecular weights of their constituent building blocks.[12] While classical theory offers a framework for targeting specific MWs via depolymerization under equilibrium control,[13] practical application is hindered by the need for long reaction times and the susceptibility of equilibrium-controlled reactions to minor environmental or compositional perturbations. Kinetic control, by contrast, provides a predictable alternative with a diverse suite of tunable parameters. Nevertheless, the vast array of input variables and the intensive labor required for traditional kinetic experiments continue to bottleneck materials discovery.

Targeting precise MWs during polymer depolymerization under kinetic control requires knowledge of how reaction rates vary over a broad range of initial reaction conditions. Mechanistic analysis is further complicated by experimental variability. Measured rate constants can differ by orders of magnitude for the same reaction due to experimental inaccuracies, human biases, or

heuristics. Further, existing kinetic datasets are often restricted to a single variable parameter (e.g., monomer concentration) and thus fail to provide sufficient information to train modern predictive models. These factors can render literature datasets insufficient or unreproducible, requiring kinetic experiments to be repeated and often producing conflicting results. Recent advancements in robotics have bolstered research productivity by automating repetitive tasks.[14-16] By integrating robotics with machine learning and AI, "self-driving laboratories" now accelerate materials discovery through autonomous experimentation. However, despite their success in other fields,[17-23] these autonomous systems remain underutilized for studying reaction kinetics and for polymer depolymerization especially.

In this contribution, we introduce an automated polymer kinetics platform implemented within the Autonomous Chemistry Laboratory (ACL), a state-of-the-art self-driving laboratory at Oak Ridge National Laboratory (ORNL). This platform enables AI-driven exploration of multi-dimensional parameter space encompassing all aspects of polymerization and depolymerization kinetic control (Figure 1). We have focused on kinetically-controlled, precision depolymerization of poly(bisphenol A carbonate) (PC) to unravel mechanistic insights and demonstrate that various MW oligomers can be readily obtained, a stark contrast to the difficulty in achieving controlled MWs via equilibrium-controlled step-growth polymerization. Using importance-guided Bayesian optimization, a probabilistic search strategy capable of handling multiple objectives,[24] our autonomous workflow with a human-in-the-loop strategically explored undersampled regions of depolymerization kinetic space to quickly determine kinetic parameters and ultimately enable the reproducible synthesis of oligomers with targeted molecular weights. Our results demonstrate a successful autonomous experimental campaign that solved the rate expression for PC depolymerization and identified the optimal design conditions for scaling up the conversion of PC

waste into value-added materials. This study represents a broader effort to exploit automation and AI to understand and control polymerization and depolymerization kinetics, and its continuous development aims to advance the field by pushing the boundaries of materials discovery.

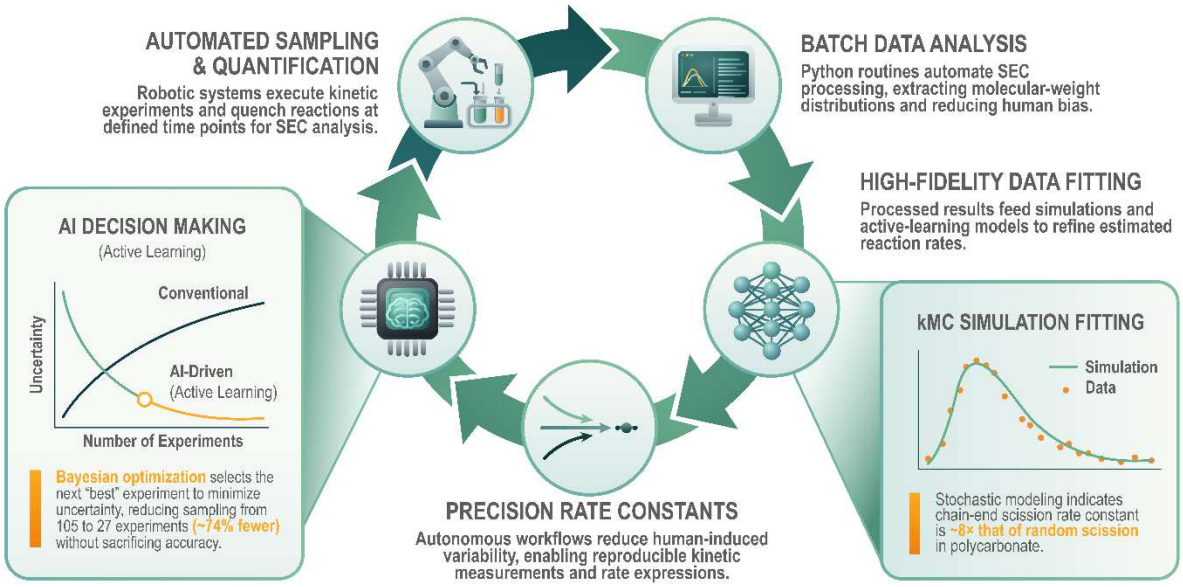


Figure 1. Automated workflow for depolymerization kinetic analysis.

Main

Initial Workflow Development

We developed an autonomous workflow that uses robotic kinetic sampling and an AI decision-making algorithm to direct future experiments. The AI algorithm could be configured to improve the reliability of kinetic predictions, reduce experimental effort, or balance both. Specific workflow steps included kinetic sampling, sample preparation, MW quantification, automated data analysis (Figure S1), data fitting with kinetic Monte Carlo (kMC) simulations (Figure S2 – S3), and AI decision making (Figure 1). As discussed below, our initial campaigns developed protocols

for automated synthesis on the ChemSpeed Swing XL robotic chemical synthesis platform and were then expanded to an AI-driven autonomous workflow with human-in-the-loop intervention.

Our first experimental campaign optimized automated kinetic sampling, replacing a tedious and error-prone manual task with a higher-throughput, more accurate, and more reproducible practice. For this initial workflow demonstration, we chose to study the glycolysis kinetics of consumer-grade PC (sourced from safety glasses), a widely available condensation thermoplastic with excellent organosolubility to facilitate homogeneous reaction monitoring. Automated PC glycolysis reactions were carried out under organocatalysis (See SD1 for further discussion). Prior to each kinetic experiment, portions of a PC/ethylene glycol (EG) stock solution were aliquoted into 20 septa-capped vials. Stock solutions of catalyst and quencher were also prepared separately in tetrahydrofuran (THF). The suite of vials was then placed in the Swing XL, and the program was initiated. During a typical automated experiment, an aliquot of the catalyst stock solution was transferred to a vial containing PC and EG to initiate depolymerization (Figure 2A). This operation was repeated for the remaining 19 vials, where each vial represented an independent reaction and thus an independent kinetic sample. At specified time points, portions of the quenching solution (containing acetic acid) were transferred to the appropriate vial to stop the reaction. After all time points had been completed, diluted samples were prepared by Swing XL for analysis (Table S1, see SD2 for expanded description of the kinetic sample sets).

During each experiment, a file containing all of the relevant metadata (i.e., time, temperature, etc.) was created; this was exported at the end of the experiment and then transferred over the control plane of ORNL's Interconnected Science Ecosystem (INTERSECT) (see SD3 for further discussion) to be used in the closed-loop, AI-driven workflow.[25-27] Each complete kinetic experiment involved a set of 21 samples (including a $t = 0$ specimen that was not included in the

Swing XL protocol) that were initiated with identical conditions but quenched at different intervals of 0 – 150 min. These samples were loaded into a size-exclusion chromatography (SEC) system and were analyzed to extract MW information and construct kinetic plots.

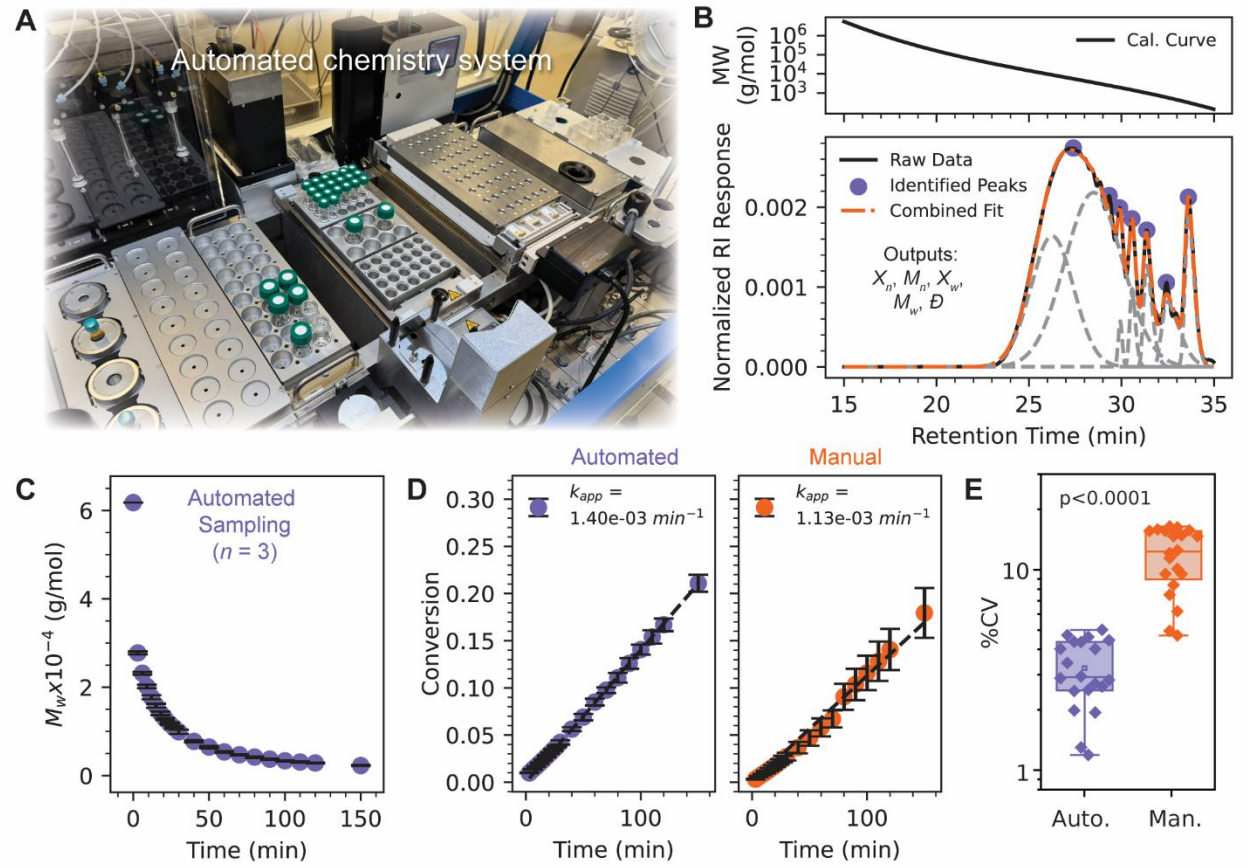


Figure 2. A) Photograph of Swing XL during a PC depolymerization experiment. B) Example output from automated SEC data analysis highlighting identified and fit peaks, the convoluted data fit, and the types of values calculated from the convolved trace using a calibration curve. C) Representative depolymerization M_w decay curve for kinetic experiment conducted by the Swing XL. D) Bond scission conversion vs time plot further emphasizing the contrast in measurement error. The dashed lines represent linear regression analyses on the two datasets. The differences in the observed slopes for the two approaches resulted in different apparent reaction rate constants despite identical reaction conditions. E) Whisker plot of the percent coefficient of variance of data collected by automated or manual experiments showing the statistically significant difference in measurement error between approaches.

Typical SEC data workup requires analysis of individual SEC chromatograms using proprietary instrument software, samplewise data exporting, and further manual data refinement

(e.g., baseline subtraction and normalization). However, the high volume of SEC data generated during our campaigns would render manual SEC analysis a significant bottleneck. To address this bottleneck, we developed an automated batch analysis routine in Python to reduce the turnaround between data collection, workup, and decision making, and to mitigate human bias associated with manual chromatograph integration (Figure 2B shows an example output, see SI for remaining outputs Figures S4 – S9). The batch analysis code used a custom metadata file generated by the Swing XL during kinetic experiments to match raw chromatographs with their appropriate sampling times and initial reaction conditions (e.g., reagent concentrations and temperature). The raw chromatographs were then subjected to baseline correction, blank subtraction, peak identification, peak fitting and fit convolution, and fit integration to calculate MW distribution averages and plot changes in MW as a function of time (Figure 2C). Outputs from batch analysis were combined with the metadata *in silico* and sent to the AI learning algorithm as observations.

To highlight the precision of automated sampling compared with traditional benchtop kinetic monitoring, we conducted PC depolymerizations either manually or using the Swing XL under otherwise identical conditions. Unsurprisingly, we observed statistically significant variance in the manual measurements (%CV = 11.34 ± 4.53) compared to those executed by the Swing XL system (%CV = 3.32 ± 1.17, Figure 2E), which we attribute to human error during the sampling process. We also observed a statistically significant difference in the time-dependent MW evolution profiles between approaches, as highlighted by the differences in slopes obtained from regression of bond scission conversion vs time plots (Figure 2D, see for conversion calculations and analysis of covariance, ANCOVA, Tables S2 – S5).

The change in inverse MW with time can be used to calculate apparent reaction rate constants using a modified Staggs equation[28]

$$\frac{M_{w,0}}{M_w} - 1 = X_{n,0} k_{app} t \quad (1)$$

where $M_{w,0}$ is the M_w at $t = 0$, $X_{n,0}$ is the number average degree of polymerization at $t = 0$, and k_{app} is the apparent reaction rate constant (see SD4 for model assumptions and discussion). Bond scission conversion is represented by the quantity $X_{n,0} k_{app} t$. Crucially, different apparent rate constants were obtained from the automated ($k_{app} = 1.40 \times 10^{-3}$ min^{-1}) and manual (1.13×10^{-3} min^{-1}) sampling experiments despite identical reaction conditions, indicating how human error could influence kinetic analysis. We point out that extra care should be taken when evaluating kinetic datasets in literature and propose that automation provides a powerful alternative for the cultivation of highly precise and reproducible kinetic data. Here, automating synthesis eliminates the 'noise' of manual execution. The highly reproducible nature of autonomous synthesis allows researchers to more easily identify the root causes of non-reproducibility, which in a robotic system are often found in the human-led upstream tasks like reagent setup.

With our partial workflow in place (automated kinetic sampling, chromatographic data collection, and automated data analysis), we conducted a series of kinetic experiments with varying initial reaction conditions. For each experiment, 21 kinetic samples were collected, keeping the quenching times consistent across a total of 26 complete kinetic runs and generating 546 individual samples (Figure 3 shows a selection of this total; see SD2 for discussion on the remainder). These in-depth kinetic experiments would normally require significant effort to conduct manually but were executed by our partial workflow with minimal human effort, offloading an estimated 82 h of human experimental time. A complete analysis of kinetic data collected via our partial workflow is provided in detail in the SI (Figures S10 – S16). In total, we observed high reproducibility and

low total measurement error for MW distribution averages and kinetic rate constants calculated across replicate experiments.

Figure 3 highlights representative kinetic observations extracted from the complete dataset. We observed first order dependencies of the reaction rate constant for PC depolymerization on both catalyst (Figure 3A) and EG (Figure 3B) concentration. Based on kinetic data collected by our "human-in-the-loop" autonomous workflow, we proposed the following rate expression for PC depolymerization in our system

$$rate = k[PC][EG][catalyst] \quad (2)$$

which is consistent with literature reports for depolymerization of related condensation polymers such as poly(ethylene terephthalate).[29, 30]

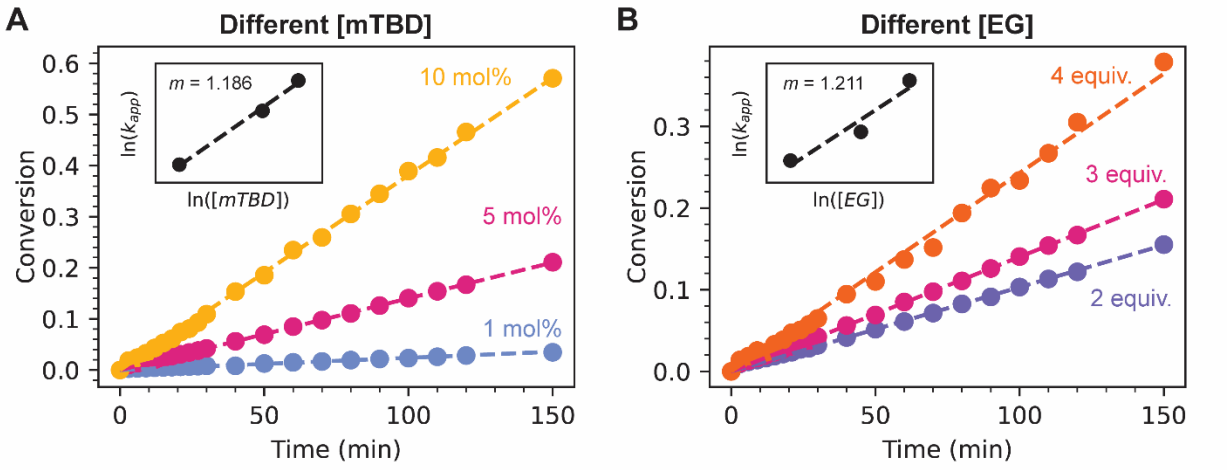


Figure 3. Representative pseudo-first order kinetic plots for PC depolymerization. Plot of conversion vs time for kinetic experiments with different initial catalyst loadings (A) or different initial concentrations of EG (B). The dashed lines represent linear fits of each sample set. The insets show double log plots of catalyst concentration (A) or EG concentration (B) vs apparent rate constants calculated using Eq 1.

Workflow Expansion with Active Learning AI

After establishing the efficacy of robotic depolymerization, the workflow was expanded to include an AI decision-making algorithm. From our initial kinetic experiments, we uncovered a first-order dependence for PC depolymerization rate on catalyst concentration as shown in Figure 3A. However, this single mechanistic determination was made via analysis of 105 samples across five complete kinetic experiments representing significant experimental and analytical effort. We hypothesized that the acquisition of this mechanistic insight could be streamlined using an active-learning AI algorithm, reducing the total number of kinetic samples required. To evaluate this hypothesis, we aimed to "rediscover" the observed first-order catalyst rate dependence using significantly fewer kinetic samples without sacrificing accuracy in rate constant calculation.

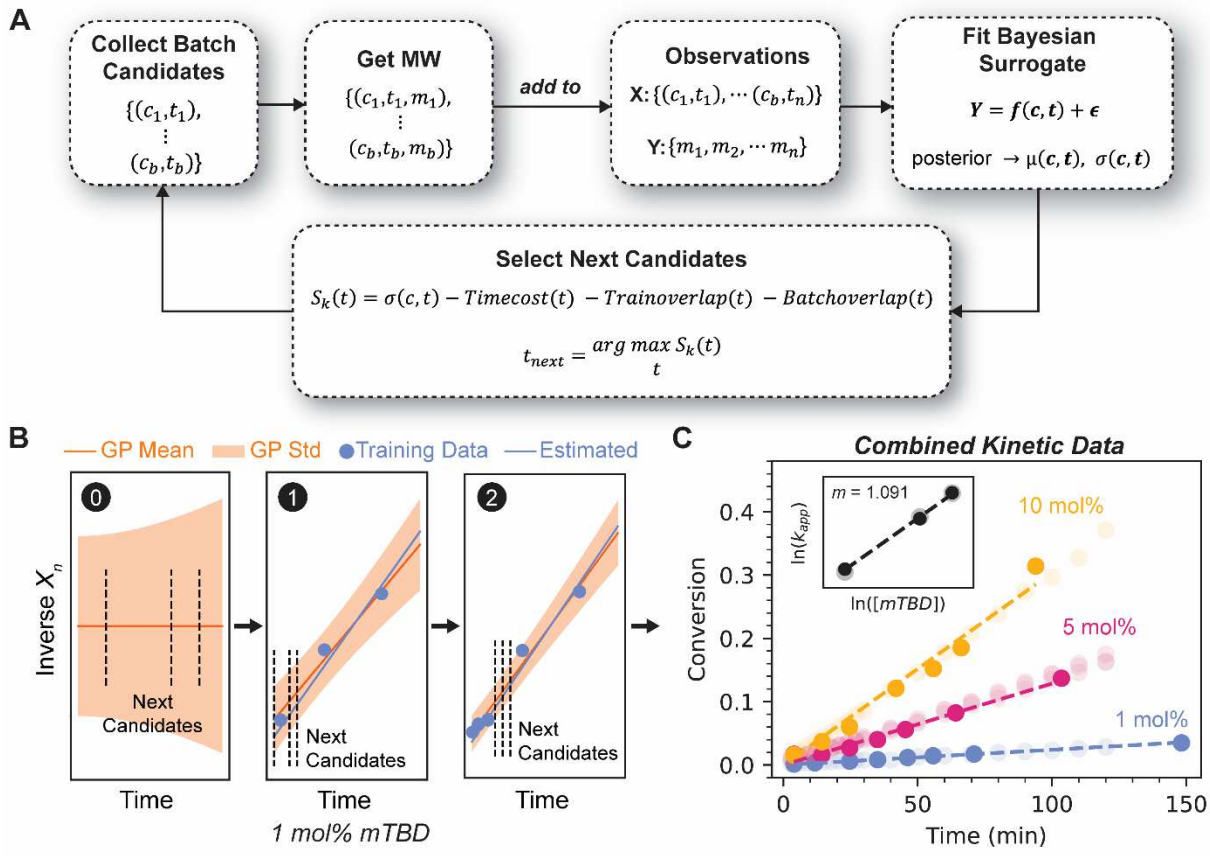


Figure 4. A) Schematic of the closed-loop active-learning workflow, where MW measurements at the corresponding catalyst concentrations and reaction times were assimilated to update the

Bayesian surrogate model, and the resulting posterior uncertainty was used within a cost-aware acquisition function to select the next batch of experiments. B) Iterative evolution of the surrogate model across active-learning cycles. The GP mean and Std represent the posterior expected prediction and associated uncertainty of the target response conditioned on the available training data. Newly acquired training data progressively refined the kinetic trend and reduced uncertainty, while the estimated regression line over the training points provided a slope-based estimate of the rate constant. C) Pseudo-first order kinetic plots of data collected at different catalyst loadings via the AI-guided workflow. New data are overlaid with data from our previous experimental campaign (translucent markers). The dashed colored lines represent linear fits of the kinetic data. The inset shows a double log plot of apparent rate constants as a function of catalyst concentration, as calculated by Eq. 1, highlighting the first-order dependence of rate on catalyst loading.

The SwingXL control, experimental data, and AI analysis systems were integrated via the control plane of INTERSECT to enable autonomous experimentation. In this workflow, SwingXL initiated testing iterations based on input variable (e.g., catalyst concentration, sampling time, etc.) files. The experimental data storage system then provided metadata to the batch analysis process and captured the results for the AI. Finally, the AI analysis system evaluated these results and transmitted parameters for the next iteration back to SwingXL. This cycle was repeated until the experimental material was exhausted or sufficient data had been collected.

To implement AI decision-making in our automated kinetic workflow, we employed a Bayesian optimization algorithm (Figure 4A). A Gaussian process (GP) surrogate model with a linear kernel was used to model observed MW parameters as a function of reaction time. The GP surrogate provided both a predictive mean and an uncertainty estimate over candidate reaction times within the range 3–200 min. New batches of reaction times were then selected by maximizing an acquisition score $S(t)$ as follows

$$S(t) = \sigma(t) - 0.01(t/100)^2 - 0.10\mathcal{P}_{\mathcal{D}}(t) - 0.10\mathcal{P}_{\mathcal{B}}(t) \quad (3)$$

where

$$\mathcal{P}_{\mathcal{D}}(t) = \max\left(0, \left(10 - \min_{t_i \in \mathcal{D}} |t - t_i|\right)/10\right) \quad (4)$$

$$\mathcal{P}_{\mathcal{B}}(t) = \max\left(0, \left(10 - \min_{t_j \in \mathcal{B}} |t - t_j|\right)/10\right) \quad (5)$$

In shown score function Eq. 3, t denotes the candidate reaction time, $\mathcal{D}$ represents the set of previously observed training times, and $\mathcal{B}$ represents the set of points already selected within the current batch. In the equation, the function $\sigma(t)$ prioritized regions of high predictive uncertainty, the second term penalized large reaction times, $\mathcal{P}_{\mathcal{D}}(t)$ penalized proximity to previously sampled conditions, and $\mathcal{P}_{\mathcal{B}}(t)$ penalized redundancy within the proposed experimental batch.

Independent Bayesian optimization loops were executed for each catalyst concentration (1, 5, and 10 mol%), and the resulting reaction time suggestions were aggregated and dispatched to the Swing XL for experimental execution (Figures S17 – S18). The measured MWs corresponding to the selected reaction times and concentrations were then assimilated with existing observations to compute the evolving kinetic trends (Figure 4B). Further, the updated dataset was used to retrain the GP surrogate model for the next iteration. This closed-loop process was repeated until the estimated kinetic rate constants converged with acceptable uncertainty.

AI-guided kinetic sampling was complete after three iterations, producing a total of 27 individual samples that were analyzed by SEC combined with our automated Python routine as described above. The linearized M_w vs time (t) curves for these samples with different catalyst loadings are shown in Figure 4C. Increased catalyst loadings resulted in depolymerization kinetics consistent with our previous observations. Apparent rate constants were extracted from the reciprocal M_w plots using Eq. 1 as described above. A strong linear correlation was obtained when

comparing k_{app} to the initial catalyst concentration (Figure 4C, inset), reinforcing our earlier observation of a first-order rate dependence on catalyst loading.

Data collected at different catalyst loadings from the AI-guided workflow were statistically compared to those collected under identical conditions during our initial experimental campaign using analysis of covariance (ANCOVA). This analysis revealed no statistically significant differences in the slopes of reciprocal M_w data collected across the two experimental campaigns despite the dramatic reduction in the number of samples collected for each (105 for the initial campaign and just 27 for the second campaign by AI-guided workflow).

To further evaluate the statistical efficiency of our autonomous experiment, we compared the confidence interval (CI) of the apparent rate constant obtained after the final autonomous campaign with fits generated by randomly selecting the same number of data points. From classical regression theory, uncertainty in slope estimation decreases more rapidly when higher reaction times are included. However, in practice, lower reaction times are often preferred for experimental convenience. To mimic this conventional approach, we randomly sub-selected observations from earlier grid-based experiments restricted to lower reaction times ($t < 50$ min). Across 20 random 8-point subsets, the 95% CI widths ranged from 0.0098 to 0.0384 (mean 0.0257), all larger than the CI obtained from the autonomous dataset (0.00924). These results demonstrated that restricting sampling to short reaction times typically increased parameter uncertainty, requiring more experiments to achieve comparable precision. Our autonomous strategy maintained this tradeoff by selectively incorporating longer-time measurements to reduce uncertainty while subsequently refining sampling in lower-time regions, thereby balancing statistical efficiency with experimental practicality. Taken together, these results confirmed our hypothesis that active-learning AI

streamlines the collection of kinetic data by reducing sample quantity without sacrificing data accuracy.

Mechanistic Insights from Simulation

To extract further mechanistic insight from kinetic data, we built a kMC simulation for polymer chain scission in Python. The simulation takes as inputs a polymer chain histogram (X_n vs frequency) generated from real experimental data and a reactivity ratio, r

$$r = \frac{k_{rand}}{k_{end}} \tag{6}$$

where k_{rand} and k_{end} are the reaction rate constants for random and chain end scission, respectively (Figure 5A). The simulation makes use of the Gillespie algorithm to stochastically sample discreet reaction events,[31] which are then executed according to rate equations S8 and S9 as described in the SI. Molecular weight distribution averages are then calculated at stipulated bond scission conversions (simply conversion, or p, below) and stored for plotting and analysis.

Figure 5B shows the average M_n decay curve from kMC simulations with $n = 5$ replicates at $r = 1 \times 10^9$ targeting a conversion of $p = 0.5$. This r value was chosen to illustrate depolymerization by exclusive random scission (i.e., $r \gg 1$). Fitting of these simulation data with the following modified form (Eq. 7) of Eq. 1.

$$\frac{M_n}{M_{n,0}} = \frac{1}{1 + (X_{n,0} - 1)p} \tag{7}$$

The analysis revealed that the kMC simulation closely agreed with the mathematical description of polymer chain scission from literature (See Appendix A in the SI). Eqs. 1 & 4 describe chain scission agnostic of the underlying depolymerization mechanism—they do not differentiate between scission occurring randomly or scission occurring predominately at chain ends. Indeed,

plotting M_n from simulations vs p for several different r produced a series of perfectly overlaid datasets (Figure S19). Thus, to capture mechanistic information a plot of M_w vs p was used instead.

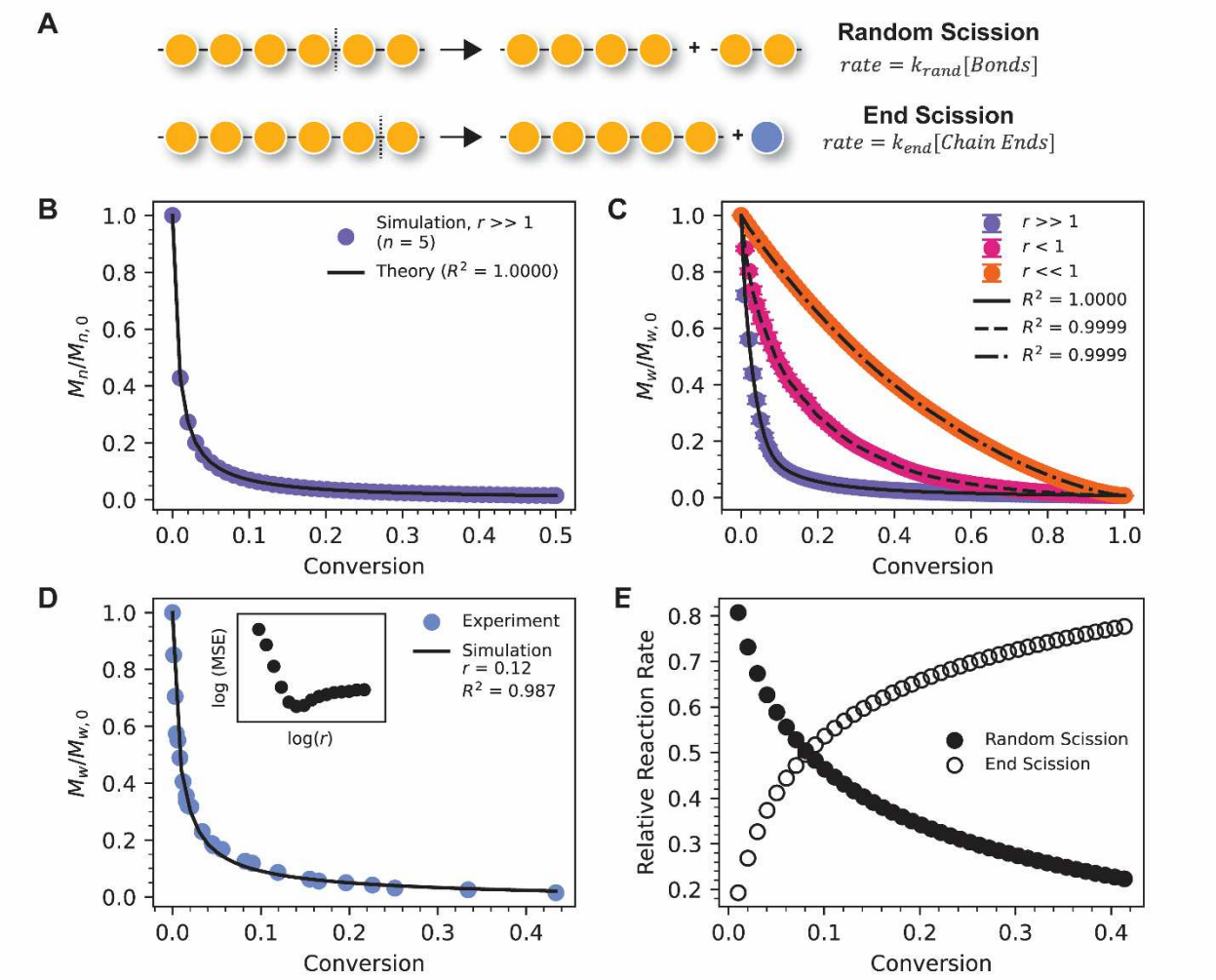


Figure 5. A) Schematic of possible polymer chain depolymerization mechanisms. B) Fit of M_n decay curve from $n = 5$ kMC simulations compared with polymer chain scission theory (Eq. 7). C) M_w decay curves for $n = 5$ kMC simulations with different r, showcasing how the chain scission mechanism influences M_w evolution during depolymerization. Data are fit with Eq. 8. D) Experimental M_w decay curve compared to simulation data. The inset shows that MSE is minimized at $r = 0.12$. E) Relative reaction rates for random scission and chain end scission as a function of conversion for a kMC simulation with $r = 0.12$.

The evolution of M_w with conversion showed stark differences for different r (Figure 5C). Here, $r = 1 \times 10^9$ ($r >> 1$) produced a decay curve with the expected reciprocal tendency, while

$r = 1 \times 10^{-9}$ ($r << 1$), or depolymerization by exclusive chain end scission, showed near-linear behavior. We fit these simulation data with a reformulation of Eq. 4 that relates conversion to M_w as follows

$$\frac{M_w}{M_{w,0}} = \frac{Đ}{Đ_0}\left[\frac{1}{1 + (X_{n,0} - 1)p}\right] \quad (8)$$

where $Đ$ and $Đ_0$ are the instantaneous and initial dispersity of the molecular weight distribution, respectively. As with the M_n data, the M_w decay curves strongly agreed with theory but also provided insight beyond theory in the form of the rate constant ratio r.

To address experimental data produced by our automated workflow with AI integration, we performed a series of simulations in which r was varied uniformly between 10^{-2} and 10^{1} and compared the simulation outputs to data from the cumulative 27 samples shown in Figure 4. These data collapsed onto a single curve when plotted as normalized M_w (relative to $t = 0$) as a function of conversion (Figure 5D), implying a common mechanism across the three kinetic experiments with different catalyst loadings. A minimum mean squared error (MSE) was obtained when comparing experimental data with the kMC simulation output corresponding to $r = 0.12$ (Figure 5D, inset). This result indicated that the rate constant for PC chain end scission in our system was approximately 8 times that of random scission. However, we note that the simulation also showed that depolymerization at low conversion was dominated by random scission events due to the starkly higher concentration of total bonds relative to bonds located at polymer chain ends (Figure 5E, Figure S20). While the physical origin of the calculated r is currently unclear, we suspect that the rate constant for random scission may exhibit a strong molecular weight dependence (i.e., $k_{rand} \propto M_n^{-a}$) as has been proposed by Gold and others.[32-34] Nevertheless, insight gained from

our kMC simulations goes beyond current literature theory and will allow us to leverage AI to finely tune depolymerization mechanism(s) in future experimental campaigns.

Physical Properties of Depolymerized PC with Precise MW Control

In addition to providing kinetic data, the reproducibility and fine control of our automated synthesis platform enabled access to highly precise oligomers as products of depolymerization (Figure 6A). Given the difficulty in synthesizing oligomers and low-MW polymers of exact MW via condensation polymerization, we envisioned that our automated depolymerization approach would provide high-quality samples to study MW-property relationships; for example, to apply the Flory-Fox relationship to PC. Moreover, while commodity PC contains unreactive *t*-butyl end-caps that prevent further chain-end growth, our glycolysis workflow furnished phenolic chain-ends that could be leveraged for downstream synthesis. Using the same autonomous protocol as above, PC oligomers of M_n 2,600 – 12000 g/mol were synthesized and isolated via precipitation. Subsequent ^{1}H NMR spectroscopic analysis (Figure S21 – S22) indicated a decrease in the proportion of *t*-butyl end-caps per polymer chain, concomitant with an increase in phenol end-groups (Figure 6B, Table S6 & Figure S23). DSC analysis revealed a linear relationship between inverse M_n and glass transition temperature, T_g, as expected for thermoplastic polymer systems (Figure 6C). Fitting these data with the Flory-Fox equation (Figure 6D), we calculated $T_{g,\infty} = 424\ \mathrm{K}$ and $K = 1.49 \times 10^5\ \mathrm{K \cdot g/mol}$, which were on the same order as literature values,[35] but likely represented a higher determination accuracy due to the broad MW range considered.

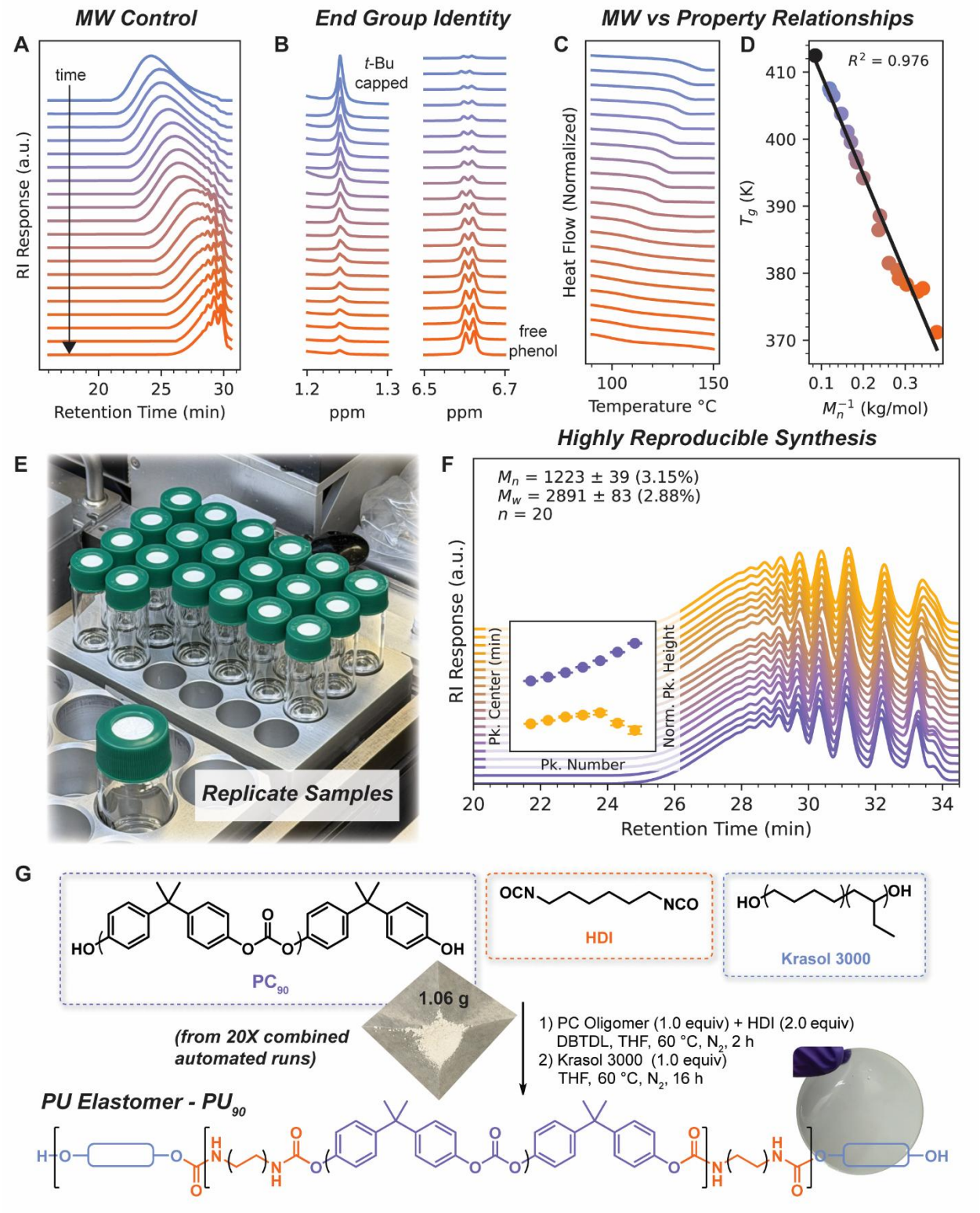


Figure 6. A) Stacked SEC chromatographs highlighting MW decay over time during depolymerization. B) Stacked slices of ^{1}H NMR spectra showing the change in relative end-group (*t*-butyl versus phenol) fractions over time. C) Stacked DSC thermograms illustrating the change

in T_g as a function MW for the PC oligomers obtained from our autonomous "human-in-the-loop" workflow. D) Flory-Fox plot of these data. MW decreases from top to bottom for A-D. E) Photograph showing the preparation of 20 samples targeting the same MW. F) Stacked SEC chromatographs highlight the reproducibility of oligomer synthesis by the Swing XL. The inset shows the consistency observed with features such as peak center and peak height. G) Scheme depicting the conversion of our precision length PC oligomer into a PU by condensing a diol-terminated polymer through urethane formation. Photographs highlight the precision **PC$_{90}$** oligomer (left) and **PU$_{90}$** polymer film (right).

The developed kinetic workflow also provided a means to "scale-up" oligomer synthesis. Automated depolymerization experiments were conducted in batches, targeting M_n = 1,000 g/mol by stopping each experiment after 90 min. SEC analysis of the crude samples revealed unprecedented consistency across a total of 20 independent syntheses (Figure 6E - F), affording an average M_n across the series of 1,223 ± 39 g/mol. The standard deviation of this dataset was nearly 1/8th of the repeat unit MW for PC, signifying very high experimental precision. Further, measured peak centers and intensities varied little across the set of 20 samples, highlighting very high similarity in their chain length distributions (Figure 6F, inset). The individual reactions were combined, isolated, and purified by precipitation yielding 1.06 g of precision oligomer **PC$_{90}$**, primed for application in further synthetic transformations.

To connect kinetic data and MW trends to synthetic applications, we sought to incorporate the **PC$_{90}$** oligomer into a new material. Oligomers such as **PC$_{90}$**, produced via glycolysis, contain phenol end-groups that are reactive (e.g., towards isocyanates in polyurethane synthesis). **PC$_{90}$** was therefore reacted with hexametheylene diisocyanate (HDI) to form an isocyanate-capped prepolymer. This prepolymer was treated with hydroxy-terminated hydrogenated polybutadiene (Krasol HLBH-P 3000) in a subsequent step to afford segmented polyurethane copolymer **PU$_{90}$** (M_n = 38,300 g/mol; Figure 6G). The desired copolymer composition was confirmed by SEC (Figure S24), ^{1}H NMR (Figure S25) and FTIR analyses (Figure S26). **PU$_{90}$** exhibited disparate properties compared to commercial PC. For example, **PU$_{90}$** possessed a low T_g at -51 °C, and a

second T_g near 100 °C, while PC exhibited a single T_g at 151 °C (Figure S27). Similarly, **PU$_{90}$** was found to thermally decompose at a lower temperature than PC (Figure S28). Tensile testing revealed **PU$_{90}$** to be a soft, highly elastic material with a Young's Modulus (E) of 1.07 ± 0.14 MPa and a tensile strain at break near 570 ± 52%, while PC exhibited a higher E of 1550 ± 72 MPa but lower strain at break of 82 ± 4.2% (Figure S29 & Table S7). Together, these results demonstrate that the precision MW oligomers produced in our autonomous campaign are primed for further synthetic transformations and show that depolymerization represents a controllable alternative to polycondensation for the synthesis of precisely defined oligomeric building blocks.

Discussion

In summary, this work establishes that the synergy of AI and automation can overcome the traditional bottlenecks of labor-intensive sampling and human-induced variability in polymer science. By integrating automated synthesis with an importance-guided Bayesian optimization algorithm, we demonstrated a workflow capable of navigating complex parameter spaces with high precision and minimal human intervention, reducing the number of needed experiments for kinetic analysis and providing access to precision oligomers. Ultimately, this autonomous framework proves that the transition from manual experimentation to AI-driven workflows not only enhances throughput but also ensures the level of accuracy required for advanced manufacturing. These results highlight the transformative potential of automation in redefining the practice of fundamental kinetic research.

Methods

Representative Polycarbonate Stock Preparation. To a 100 mL round-bottom flask equipped with a stir bar, 77 mL of THF were added. The flask was submerged in an oil bath heated to 40 °C, followed by a gradual addition of 2.2 g (8.65 mmol) of PC pieces (sourced from safety glasses) over the course of approximately 5 hours. Upon complete dissolution, the stock solution was allowed to cool to room temperature.

Representative Autonomously Aided PC Deconstruction. Stock solutions of quencher AcOH (0.4 M) and catalyst mTBD (0.03 M) were prepared in separate 20 mL scintillation vials with septa caps. A stock solution of PC was prepared as described above. Upon cooling to room temperature, EG (1.45 mL) was added dropwise to the PC stock solution with vigorous stirring. An initial t_0 aliquot (3.5 mL) was collected from the stock and added to a 2-dram vial in the absence of AcOH. Twenty-two-dram vials were then filled with 3.5 mL of the PC:EG stock each and placed into a 24-vial reaction block. A separate 24-vial reaction block was filled with empty septa-capped 1-dram vials, and then both reaction blocks and AcOH and mTBD stocks were transferred into the ChemSpeed Swing XL system.

ChemSpeed Swing XL Workflow. A Chemspeed Autosuite file was written to control the Swing XL within the Autonomous Chemistry Laboratory (ACL) at Oak Ridge National Laboratory (ORNL). The 4-needle-head was used to transfer liquids in the range of 0.2 to 0.8 mL, including the transfer of 0.5mL of catalyst stock solution to initiate each depolymerization, and the transfer of 0.5mL of the acetic acid stock solution for quenching the reaction. Reaction times were calculated from the endpoint of the catalyst transfer to the endpoint of the quenching agent in the workflow. In each campaign, kinetic sampling was conducted initially over a predefined set of times for 20 samples, with times ranging from 3 minutes to 30 minutes in 3-minute intervals, followed by 40 minutes to 120 minutes in 10-minute intervals, and finally at 150 minutes. The temperature was controlled to within a 0.1 degree variation for the sample, catalyst and quenching agent source vials, at 25.0 ^{o}C. The transfer volume was calibrated by dispensing a series of volumes from 0.2 to 0.8 mL at 3 mL/minute (as used in the kinetic sampling experiments), followed by measuring the dispensed mass and comparing against the calculated mass for the known solvent density (THF). The dispensed volumes were then corrected for offsets, typically found to be within approximately 3 % or less deviation from the expected value. All reactions were conducted in two-dram glass vials

with septa caps. Metadata were exported according to the process described in **SD3**. Each campaign was initiated using a formatted text file containing suggested reaction parameters that were generated by the surrogate model.

Materials: Poly(bisphenol A carbonate) (PC) safety-glasses (M_n ~ 35 kDa, M_w ~ 65,000 g/mol, PDI ~ 1.9) were acquired from VWR Chemicals and broken into small chunks (approximately 0.05 g each) using small wire cutters. 7-methyl-1,5,7-triazabicylco(4.4.0)dec-5-ene (mTBD), was acquired from Ambeed and used without further purification. Ethylene glycol (EG), hexamethylenediisocyante (HDI), and dibutyltin dilaurate (DBTDL) were acquired from Sigma-Aldrich and used without further purification. Hydroxy-terminated hydrogenated polybutadiene (PBD) (Krasol® HLBH-P 3000) was provided by Cray Valley chemicals and used without further purification. Tetrahydrofuran (stabilized with 200-300 ppm BHT) and other solvents were acquired from VWR Chemicals and used as received.

Supporting Information

The supporting information is available free of charge. All experimental details, characterization data, and additional kinetic data are described in the supporting information.

Author Contributions

NJG: Conceptualization, Methodology, Investigation, Writing – original draft and reviewing/editing. **BB**: Investigation, Writing – reviewing and editing. **JK**: Investigation. **BY**: Investigation. **NO**: Investigation. **ID**: Investigation. **JB**: Investigation. **JM**: Software, Writing – reviewing and editing. **AS**: Software, Writing – reviewing and editing. **SDeWitt**: Software, Writing – reviewing and editing, Funding Acquisition. **SDai**: Conceptualization, Funding Acquisition. **CB**: Conceptualization, Methodology, Investigation, Writing – reviewing and editing,

Funding Acquisition. **JF**: Conceptualization, Methodology, Software, Formal Analysis, Writing – original draft and reviewing/editing, Visualization, Supervision, Funding Acquisition. **TS**: Conceptualization, Methodology, Writing – original draft and reviewing/editing, Supervision, Funding Acquisition.

Competing Interests

The authors declare no competing financial interests.

Acknowledgments

This research was supported by the U.S. Department of Energy, Office of Science, Basic Energy Sciences, Materials Sciences and Engineering Division. ACL at ORNL, along with autonomous synthesis operation and AI-incorporation in this study were supported by the INTERSECT initiative as a part of the Laboratory Directed Research and Development Program of Oak Ridge National Laboratory. This research used resources from the ORNL Research Cloud Infrastructure at the Oak Ridge National Laboratory, which is supported by the Office of Science of the U.S. Department of Energy under Contract No. DE-AC05-00OR22725.

References

(1) Chittari, S. S.; Dykeman-Bermingham, P. A.; Bogen, M. P.; Knight, A. S. Structure–Function Insights into Thermoresponsive Copolymers as Lanthanide Precipitants. *Journal of the American Chemical Society* **146** (49) (2024).

(2) Bogen, M. P.; Swofford, W. M.; Chittari, S. S.; Knight, A. S. Structure–Function Relationships in Sequence-Controlled Copolymers for Rare Earth Element Chelation. *Journal of the American Chemical Society* **147** , 30885-30896 (2025).

(3) Gallagher, C. M. B.; Schulz, M. D. Effect of Ionic Strength and Anion Identity on Rare-Earth Element Chelation by Poly(acrylic acid). *Macromolecular Chemistry and Physics* **224**, 2300235 (2023).

(4) Archer, W. R.; Chen, T.; Vaissier Welborn, V.; Schulz, M. D. Polymer Tacticity Effects in Polymer–Lanthanide Chelation Thermodynamics. *Macromolecules* **56**, 9062-9069 (2023).

(5) Rapp, J. L.; Borden, M. A.; Bhat, V.; Sarabia, A.; Leibfarth, F. A. Continuous Polymer Synthesis and Manufacturing of Polyurethane Elastomers Enabled by Automation. *ACS Polymers Au* **4**, 120-127 (2024).

(6) Rapp, J. L.; Anstine, D. M.; Gusev, F.; Nikitin, F.; Yun, K. H.; Borden, M. A.; Bhat, V.; Isayev, O.; Leibfarth, F. A. Design of Tough 3D Printable Elastomers with Human-in-the-Loop Reinforcement Learning. *Angewandte Chemie International Edition* **64**, e202513147 (2025).

(7) Kozuszek, C. T.; Sorensen, C. C.; Leibfarth, F. A. Understanding and Enhancing Stereoselective Polymerization Using a Data Science Approach. *Journal of the American Chemical Society* **147**, 45914-45923 (2025).

(8) Röttger, M.; Domenech, T.; van der Weegen, R.; Breuillac, A.; Nicolaÿ, R.; Leibler, L. High-performance vitrimers from commodity thermoplastics through dioxaborolane metathesis. *Science* **356**, 62-65 (2017).

(9) Danielson, M. K.; Gainaru, C.; Demchuk, Z.; Pan, C.; Choi, J.; Zhang, H.-H.; Foster, J. C.; Saito, T.; Rahman, M. A. Closed-Loop Recyclable Vitrimer Plastics from PET Waste: A Design for Circularity. *ChemSusChem* **18**, e202500898 (2025).

(10) Zheng, J.; Galan, N. J.; Boucher, M.; Jupp, O.; Karunarathna, M. S.; Choi, J.; Kehelkadu Withanage, C. C. M.; Nelson, T. L.; Foster, J. C.; Saito, T. Tailored glycolysis of Nylon 6 to enable upcycling into high-strength adhesives. *Cell Reports Physical Science* **6** (2025).

(11) Galan, N. J.; Dishner, I. T.; Sumpter, B. G.; Kertesz, V.; Abdul Rahman, N. B.; Polo-Garzon, F.; Demchuk, Z.; Saito, T.; Foster, J. C. Upcycling of polyethylene terephthalate to high-value chemicals by carbonate-interchange deconstruction. *Green Chemistry* **27**, 10.1039/D5GC03354C (2025).

(12) Guselnikova, O.; Semyonov, O.; Sviridova, E.; Gulyaev, R.; Gorbunova, A.; Kogolev, D.; Trelin, A.; Yamauchi, Y.; Boukherroub, R.; Postnikov, P. "Functional upcycling" of polymer waste towards the design of new materials. *Chemical Society Reviews* **52**, 4755-4832 (2023).

(13) Meaurio, E. Generalization of the Carothers equation for linear step growth polymers. *Scientific Reports* **14**, 27281 (2024).

(14) Burger, B.; Maffettone, P. M.; Gusev, V. V.; Aitchison, C. M.; Bai, Y.; Wang, X.; Li, X.; Alston, B. M.; Li, B.; Clowes, R.; et al. A mobile robotic chemist. *Nature* **583**, 237-241 (2020).
(15) Dai, T.; Vijayakrishnan, S.; Szczypiński, F. T.; Ayme, J.-F.; Simaei, E.; Fellowes, T.; Clowes, R.; Kotopanov, L.; Shields, C. E.; Zhou, Z.; et al. Autonomous mobile robots for exploratory synthetic chemistry. *Nature* **635**, 890-897 (2024).
(16) Lunt, A. M.; Fakhruldeen, H.; Pizzuto, G.; Longley, L.; White, A.; Rankin, N.; Clowes, R.; Alston, B.; Gigli, L.; Day, G. M.; et al. Modular, multi-robot integration of laboratories: an autonomous workflow for solid-state chemistry. *Chemical Science* **15**, 2456-2463 (2024).
(17) Murphy, E. A.; Roth, K. G.; Bates, M. W.; Murphy, M. C.; Edmund, J.; Bates, C. M.; Hawker, C. J. High-Throughput Generation of Block Copolymer Libraries via Click Chemistry and Automated Chromatography. *Macromolecules* **58**, 8369-8376 (2025).
(18) Angello, N. H.; Rathore, V.; Beker, W.; Wołos, A.; Jira, E. R.; Roszak, R.; Wu, T. C.; Schroeder, C. M.; Aspuru-Guzik, A.; Grzybowski, B. A.; et al. Closed-loop optimization of general reaction conditions for heteroaryl Suzuki-Miyaura coupling. *Science* **378**, 399-405 (2022).
(19) Jafari, V. F.; Mossayebi, Z.; Allison-Logan, S.; Shabani, S.; Qiao, G. G. The Power of Automation in Polymer Chemistry: Precision Synthesis of Multiblock Copolymers with Block Sequence Control. *Chemistry – A European Journal* **29**, e202301767 (2023).
(20) Lee, J.; Mulay, P.; Tamasi, M. J.; Yeow, J.; Stevens, M. M.; Gormley, A. J. A fully automated platform for photoinitiated RAFT polymerization. *Digital Discovery* **2**, 219-233, (2023).
(21) Szymanski, N. J.; Rendy, B.; Fei, Y.; Kumar, R. E.; He, T.; Milsted, D.; McDermott, M. J.; Gallant, M.; Cubuk, E. D.; Merchant, A.; et al. An autonomous laboratory for the accelerated synthesis of novel materials. *Nature* **624,** 86-91 (2023).
(22) Beaucage, P. A.; Sutherland, D. R.; Martin, T. B. Automation and Machine Learning for Accelerated Polymer Characterization and Development: Past, Potential, and a Path Forward. *Macromolecules* **57**, 8661-8670 (2024).
(23) Knox, S. T.; Wu, K. E.; Islam, N.; O'Connell, R.; Pittaway, P. M.; Chingono, K. E.; Oyekan, J.; Panoutsos, G.; Chamberlain, T. W.; Bourne, R. A.; et al. Self-driving laboratory platform for many-objective self-optimisation of polymer nanoparticle synthesis with cloud-integrated machine learning and orthogonal online analytics. *Polymer Chemistry* **16**, 1355-1364 (2025).
(24) Shrivastava, A.; Kalaswad, M.; Custer, J. O.; Adams, D. P.; Najm, H. N. Bayesian optimization for stable properties amid processing fluctuations in sputter deposition. *Journal of Vacuum Science & Technology A* **42**, 033408 (2024).
(25) Thakur, A. M.; Hitefield, S.; McDonnell, M.; Wolf, M.; Archibald, R.; Drane, L.; Roccapriore, K.; Ziatdinov, M.; McGaha, J.; Smith, R.; et al. Towards a Software Development Framework for Interconnected Science Ecosystems. In *Accelerating Science and Engineering Discoveries Through Integrated Research Infrastructure for Experiment, Big Data, Modeling and Simulation*, Cham, 2022//, 2022; Doug, K., Al, G., Pophale, S., Liu, H., Parete-Koon, S., Eds.; Springer Nature Switzerland: pp 206-224.

(26) *INTERSECT Architecture Documentation*; github, https://intersect-architecture.readthedocs.io.
(27) *INTERSECT-DIAL/dial: Dial v0.1*; Zenodo: Zenodo, 2025. https://doi.org/10.5281/zenodo.14872254.
(28) Staggs, J. E. J. Modelling random scission of linear polymers. *Polymer Degradation and Stability* **76**, 37-44 (2002).
(29) Sangalang, A.; Bartolome, L.; Kim, D. H. Generalized kinetic analysis of heterogeneous PET glycolysis: Nucleation-controlled depolymerization. *Polymer Degradation and Stability* **115**, 45-53 (2015).
(30) Chen, J.-W.; Chen, L.-W.; Cheng, W.-H. Kinetics of glycolysis of polyethylene terephthalate with zinc catalyst. *Polymer International* **48**, 885-888 (1999).
(31) Gillespie, D. T. Exact stochastic simulation of coupled chemical reactions. *The Journal of Physical Chemistry* **81**, 2340-2361 (1977).
(32) Gold, L. Variable Reaction Rate Theory of Polymer Size Distribution. *The Journal of Chemical Physics* **30,** 1284-1286 (1959).
(33) Nanda, V. S.; Jain, S. C. Effect of Variation of the Bimolecular Rate Constant with Chain Length on the Statistical Character of Condensation Polymers. *The Journal of Chemical Physics* **49**, 1318-1320 (1968).
(34) Orlova, T. M.; Pavlova, S. S. A.; Dubrovina, L. V. Statistical approach to the molecular weight distribution of condensation polymers. *Journal of Polymer Science: Polymer Chemistry Edition* **17**, 2209-2221 (1979).
(35) Cheah, K.; Cook, W. D. Structure-property relationships of blends of polycarbonate. *Polymer Engineering & Science* **43**, 1727-1739 (2003).

Supplementary Files

This is a list of supplementary files associated with this preprint. Click to download.

- ACLSINatureSubmission.pdf